Title
Catalytic proton reduction with transition metal complexes of the redox-active ligand bpy2PYMe

Journal
Chemical Science, 4(10)

ISSN
2041-6520

Authors
Nippe, Michael
Khnayzer, Rony S
Panetier, Julien A
et al.

Publication Date
2013

DOI
10.1039/c3sc51660a

Peer reviewed

Chemical Science

RSC Publishing

EDGE ARTICLE

View Article Online
View Journal | View Issue

Cite this: *Chem. Sci.*, 2013, **4**, 3934

Catalytic proton reduction with transition metal complexes of the redox-active ligand bpy2PYMe†

Michael Nippe,[ab] Rony S. Khnayzer,[c] Julien A. Panetier,[ab] David Z. Zee,[ab] Babatunde S. Olaiya,[c] Martin Head-Gordon,[ad] Christopher J. Chang,*[adef] Felix N. Castellano*[c] and Jeffrey R. Long*[ab]

A new pentadentate, redox-active ligand **bpy2PYMe** has been synthesized and its corresponding transition metal complexes of Fe^{2+} (**1**), Co^{2+} (**2**), Ni^{2+} (**3**), Cu^{2+} (**4**), and Zn^{2+} (**5**) have been investigated for electro- and photo-catalytic proton reduction in acetonitrile and water, respectively. Under weak acid conditions, the Co complex displays catalytic onset at potentials similar to those of the ligand centered reductions in the absence of acid. Related Co complexes devoid of ligand redox activity catalyze H_2 evolution under similar conditions at significantly higher overpotentials, showcasing the beneficial effect of combining ligand-centered redox activity with a redox-active Co center. Furthermore, turnover numbers as high as 1630 could be obtained under aqueous photocatalytic conditions using $[Ru(bpy)_3]^{2+}$ as a photosensitizer. Under those conditions catalytic hydrogen production was solely limited by photosensitizer stability. Introduction of an electron withdrawing CF_3 group into the pyridine moiety of the ligand as in **bpy2PYMe-CF$_3$** renders its corresponding Co complex **6** less active for proton reduction in electro- and photocatalytic experiments. This surprising effect of ligand substitution was investigated by means of density functional theory calculations which suggest the importance of electronic communication between Co^{1+} and the redox-active ligand. Taken together, the results provide a path forward in the design of robust molecular catalysts in aqueous media with minimized overpotential by exploiting the synergy between redox-active metal and ligand components.

Received 13th June 2013
Accepted 7th August 2013

DOI: 10.1039/c3sc51660a

www.rsc.org/chemicalscience

Introduction

Molecular systems capable of utilizing electrons (or electron–holes) from an electrode or semiconductor for catalysis of energy-relevant chemical conversions, such as proton or CO_2 reduction or water oxidation, are rightfully attracting increased attention, as they constitute an essential component for the efficient conversion of solar energy into chemical energy.[1] Electrocatalytic H_2 evolution has been reported for a variety of earth abundant transition metal complexes in organic solvents[2,3] as well as in aqueous media.[4] In particular, Co and Ni complexes have been the subject of catalytic studies, and while mechanistic details for turnover relevant species have been investigated,[5] a consensus has not been reached for most Co complexes. It is, however, widely established that certain Co hydride species are necessary to enter the catalytic cycle and therefore a discussion of the conditions leading to such species is appropriate.

Most studies of proton reduction catalysis by Co complexes have been performed in organic solvents utilizing strong acids as proton sources, that is, acids with thermodynamic potentials (E^0_{SAH})[6] positive of the initial Co(II/I) redox couple. Under such conditions, protonation of transient Co(I) to yield Co(III)–H species is efficient and the latter species enter the catalytic cycle to evolve H_2 by either mono- or dinuclear pathways, giving rise to a catalytic current at potentials slightly positive of the Co(II/I) potential (red trace in Scheme 1). In contrast, electrocatalytic proton reduction by Co complexes in aqueous media is typically preceded by other reductive events, suggesting that formation of lower valent Co species is necessary for catalysis and that the

[a]*Department of Chemistry, University of California, Berkeley, California 94720, USA*
[b]*Materials Sciences Division and Chemical Sciences Division, Lawrence Berkeley National Laboratory, Berkeley, California 94720, USA*
[c]*Department of Chemistry and Center for Photochemical Sciences, Bowling Green State University, Bowling Green, Ohio 43403, USA*
[d]*Chemical Sciences Division, Lawrence Berkeley National Laboratory, Berkeley, California 94720, USA*
[e]*Howard Hughes Medical Institute, University of California, Berkeley, California 94720, USA. E-mail: chrischang@berkeley.edu; jrlong@berkeley.edu; castell@bgsu.edu*
[f]*Department of Molecular and Cell Biology, University of California, Berkeley, California 94720, USA*

† Electronic supplementary information (ESI) available: Molecular structures of **1**, **3**, **4**, **5**; crystallographic information and bond lengths; UV/Vis and EPR spectra; DC magnetic susceptibility data for **2**; pH, concentration dependence of $[Ru(bpy)_3]^{2+}$ and ascorbic acid of photocatalytic H_2 production; photoluminescence quenching of $[Ru(bpy)_3]^{2+}$; computational information. CCDC 943488–943492. For ESI and crystallographic data in CIF or other electronic format see DOI: 10.1039/c3sc51660a

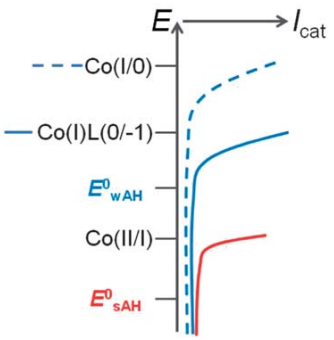

Scheme 1 Relation of acid strength to redox potentials of Co based HER catalyst.

observed catalytic current enhancements do not involve the Co(I)/Co(III)–H pathway.

A similar situation presents itself for proton reduction by Co complexes utilizing weak organic acids (with E^0_{wAH} more negative than the Co(II/I) redox couple). Protonation of Co(I) is therein not efficient and catalytic currents are expected to be caused by protonation of Co(0) to yield Co(II)–H species (blue dashed trace in Scheme 1).

This may contribute to the high overpotentials typically obtained for Co complexes in water. One approach to lowering these overpotentials would be to introduce another redox event with a potential intermediate to the Co(II/I) and Co(I/0) couples. Such an additional reduction could possibly be achieved by utilizing appropriate redox-active ligands. If ligand reduction to Co(I)L() results in a catalytically competent species, catalytic current positive of the ligand centered reduction would be anticipated (solid blue trace in Scheme 1), resulting in a significantly lowered overpotential.

Precedence for catalytic systems which combine redox-active metal centers with redox-active ligand moieties,[7] such as porphyrins,[8] phthalocyanines,[9] and dithiolenes,[10] do exist but it is only recently that directed attempts have been made to exploit the interplay of ligand and metal redox-activity for electrocatalytic proton reduction.[11] Crabtree and coworkers recently reported a Ni(II) complex with the NNN pincer ligand shown in Scheme 2 to be active for proton reduction in acetonitrile and aqueous media.[12] Results from density functional theory (DFT) calculations and EPR spectroscopy suggest initial one-electron ligand reduction to yield a (L)Ni(II) species, which concomitantly undergoes proton coupled electron transfer (PCET) to form a LNi(II)–H species that is protonated, thereby yielding an LNi(II)–H_2 intermediate. Similar initial ligand reduction had earlier been reported by the same group for a closely related Ni(II) complex with a tetradentate macrocyclic ligand, although a (L)Ni(III)–H intermediate was proposed in that case.[13] Another example is given by a Co(II) complex of a bis(iminopyridine) ligand (Scheme 2) which shows strongly pH dependent electrochemical signatures.[14] In contrast to the above described Ni(NNN) example, the initial reduction is metal based, yielding a (L)Co(I) complex. Subsequent one-electron reduction furnishes supposedly a (L)Co(I) species, which can then react with protons through various pathways that need further investigation. It should be noted that both of the aforementioned catalysts utilize ligands with unsaturated imino functional groups. Importantly, closely related oxime functional groups in Co catalysts bearing bisglyoxime[15] and trisglyoxime[16] ligand sets (Scheme 2) are likely to or have been shown to undergo hydrogenation[17] during catalysis.

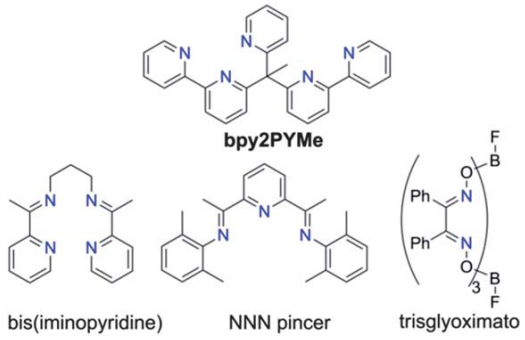

Scheme 2 Redox active ligands utilized in HER catalysis.

The present work was inspired by early findings that $[Co(bpy)_3]^+$ (bpy = 2,2′-bipyridine), which displays a strongly delocalized electronic structure[18] and could likely involve redox-activity of the bpy ligands for catalysis, reacts with protons to produce H_2,[19] and has frequently been used as a precatalyst in photocatalytic experiments for H_2 evolution.[20] Therefore we designed the new ligand **bpy2PYMe** (Scheme 2), which incorporates two redox-active bpy moieties that are expected to be stable towards ligand hydrogenation. Furthermore, the pentadentate nature of **bpy2PYMe** is expected to benefit catalyst stability (as compared to $[Co(bpy)_3]^{n+}$) and the π accepting properties of bpy to result in more positive reduction potentials for the metal center (as compared to pure pyridine ligand sets such as $PY5Me_2$; $PY5Me_2$ = 2,6-bis(1,1-di-2-pyridinylethyl)-pyridine). Here, we report the **bpy2PYMe** complexes of Fe(II) (**1**), Co(II) (**2**), Ni(II) (**3**), Cu(II) (**4**), and Zn(II) (**5**) and a systematic comparison of their structural and electrochemical properties. Complex **2** displays the highest electrocatalytic activity in acetonitrile if the weak acid acetic acid is the proton source. Importantly, catalytic onset is observed at potentials that match well with the ligand based reduction events in the absence of acid. The earlier published pyridine Co complex $[Co(CF_3)PY5Me_2(CH_3CN)]^{2+}$,[4d] which is lacking such ligand redox activity, reduces protons at more negative potentials. Additionally, visible-light energized homogeneous H_2 evolution experiments in water using **2** in conjunction with $[Ru(bpy)_3]^{2+}$ and ascorbate[19c,21] displays impressive photocatalysis metrics. Our findings suggest that ligand redox activity can improve electrocatalytic performance of Co complexes and have important implications for other Co catalysts for which such pathways have not been considered.[22]

Experimental section

Materials and methods

The compounds 2-ethylpyridine, 6-bromo-2,2′-bipyridine, $AgCF_3SO_3$, $Cu(CF_3SO_3)_2$, $Ni(BF_4)_2$, butyllithium, methyllithium,

diisopropylamine, ethylmagnesium bromide, $Fe(acac)_3$, tris(2,2′-bipyridyl)dichlororuthenium(II) hexahydrate ($Ru(bpy)_3Cl_2 \cdot 6H_2O$), and L-ascorbic acid were purchased from Sigma-Aldrich, and NBu_4PF_6 (Strem), $Fe(CF_3SO_3)_2$ (Wako), $ZnCl_2$ (Strem), 2-chloro-4-trifluoromethylpyridine (Oakwood Chemicals) were purchased from other sources. Infrared spectra were obtained on a Nicolet Avatar 360 FTIR spectrometer equipped with an attenuated total reflectance (ATR) accessory. Carbon, hydrogen, and nitrogen analyses were obtained from the Microanalytical Laboratory at the University of California, Berkeley. ^{1}H, ^{13}C, and ^{19}F-NMR spectra were obtained using either a Bruker AVQ-400, AVB-300, or AVANCEIII 500 instrument and peaks were referenced to residual solvent peaks. Positive mode electrospray ionization mass spectrometry (ESI-MS) measurements were performed using a quadrupole time-of-flight mass spectrometer (Q-tof Premier, Waters, Milford, MA). High-resolution mass spectrometry (HRMS) measurements were performed using an Autospec mass spectrometer (Waters). UV/Vis spectra were acquired on a Shimadzu SolidSpec-3700 (Fig. S9†). X-band EPR spectra of **4** (Fig. S6†) were acquired using a Bruker ELEXSYS. Magnetic data of **2** (Fig. S7†) were collected on a Quantum Design MPMS-XL SQUID magnetometer. Cyclic voltammograms were recorded using a BASi CV-50W potentiostat and a three electrode setup, with glassy carbon disk (working), Pt-wire or carbon rod (auxiliary), and Ag/AgCl (aq) or $Ag/AgPF_6$ (non-aq) electrode (reference). The ferrocene/ferrocenium couple was used as an internal standard. Electrolysis was performed using a two-compartment cell with a calibrated non-aqueous $Ag/AgPF_6$ reference electrode and a glassy carbon rod working electrode in one compartment, separated by a porous glass frit from a second compartment with a graphite rod auxiliary electrode. Determination of the quantity of H_2 evolved during electrolysis was achieved *via* gas chromatography measurements with a calibration curve, for which 5 mL of methane was injected as an internal standard.[23]

Syntheses

bpy2PYMe. The precursor molecule 1-(2-pyridyl)-1-(6-2,2′-bipyridyl)ethane was synthesized as follows. Methyllithium (1.6 M in diethyl ether, 8.06 mL, 12.9 mmol) was added to a solution of 2-ethylpyridine (1.53 mL, 12.9 mmol) in THF (100 mL) at −78 °C. The stirred mixture was slowly warmed to 0 °C and stirring was continued at this temperature for 1 h during which the mixture turned red. A solution of 6-bromo-2,2′-bipyridine (2.02 g, 8.59 mmol) in THF (40 mL) was added and the mixture was allowed to stir at room temperature for 48 h. The reaction was quenched with H_2O (40 mL) and the product was extracted with CH_2Cl_2 (3 × 80 mL) and the combined organics dried over $MgSO_4$. After filtration and solvent removal the sticky pale yellow solid was dissolved in a minimum amount of CH_2Cl_2 to which hexanes were added until the mixture appeared cloudy and was stored at 0 °C for 12 h. After filtration and solvent removal 1-(2-pyridyl)-1-(6-2,2′-bipyridyl)ethane was obtained in yields exceeding 90% with 96% purity, as determined by NMR spectroscopy (the impurity is **bpy2PYMe**) and used for the synthesis of **bpy2PYMe**. ^{1}H-NMR ($CDCl_3$, 500 MHz, ppm): δ 8.65 (1H, d), 8.57 (1H, d), 8.49 (1H, d), 8.47 (1H, d), 8.23 (1H, d), 7.79 (1H, t), 7.71 (1H, t), 7.59 (1H, t), 7.35 (1H, d), 7.27 (1H, t), 7.12 (1H, d), 4.55 (1H, q), 1.83 (3H, d). ^{13}C-NMR ($CDCl_3$, 126 MHz, ppm): δ 164.2, 163.0, 156.5, 155.2, 149.1, 149.0, 137.3, 136.8, 136.4, 123.5, 122.6, 122.5, 121.4, 121.2, 118.6, 49.9, 19.9. Next, butyllithium (2.5 M in hexanes, 3.46 mL, 8.65 mmol) was added to 1-(2-pyridyl)-1-(6-2,2′-bipyridyl)ethane (2.26 g, 8.65 mmol) at 0 °C and stirring was continued for 50 min at this temperature after which a solution of 6-bromo-2,2′-bipyridine (2.24 g, 9.51 mmol) in THF (30 mL) was added and the mixture was allowed to warm to room temperature. After stirring at reflux for 14 h, the mixture was cooled to room temperature, quenched with H_2O (80 mL), and extracted with CH_2Cl_2 (3 × 100 mL). After drying the combined organics ($MgSO_4$) and solvent removal under reduced pressure the product was purified by column chromatography (silica, 1st CH_2Cl_2, 2nd EtOAc). Yield: 2.87 g (80%). Anal. calcd for $C_{27}H_{21}N_5$: C, 78.05%; H, 5.09%; N, 16.86%. Found: C, 77.62%; H, 4.99%; N, 16.56%. ^{1}H-NMR ($CDCl_3$, 400 MHz, ppm): δ 8.62 (3H, d), 8.27 (2H, d), 8.20 (2H, d), 7.73 (2H, t), 7.68 (2H, d), 7.57 (1H, t), 7.24 (1H, d), 7.22 (1H, d), 7.19 (2H, d), 7.13 (2H, m), 2.51 (3H, s). ^{13}C-NMR ($CDCl_3$, 126 MHz, ppm): δ 166.4, 165.0, 156.5, 154.5, 148.9, 148.7, 136,8, 136.7, 135.7, 123.9, 123.8, 123.5, 121.3, 121.1, 118.2, 60.5, 27.1. IR (neat, cm^{-1}): 1733 (w), 1579 (s), 1560 (s), 1498 (w), 1470 (m), 1453 (m), 1424 (s), 1366 (w), 1286 (w), 1259 (m), 1196 (vw), 1150 (m), 1117 (m), 1066 (m), 1090 (m), 1042 (m), 990 (s), 898 (w), 826 (w), 772 (s), 746 (s), 722 (w), 698 (w), 674 (m), 665 (m), 629 (m), 619 (s), 561 (w), 540 (m), 511 (w).

2-Ethyl-4-trifluoromethylpyridine. Ethylmagnesium bromide (3.0 M in Et_2O, 23.9 mL, 71.6 mmol) was slowly added to a 500 mL Schlenk flask containing a stirred solution of iron(III) acetylacetonate (973 mg, 2.76 mmol) and 2-chloro-4-trifluoromethylpyridine (7.09 mL, 55.1 mmol) in a mixture of THF (275 mL) and *N*-methyl-2-pyrrolidone (25 mL) at 0 °C. The resulting dark violet solution was allowed to warm to room temperature and stirred for an additional 20 min before quenching with 200 mL of saturated aqueous NH_4Cl. The aqueous and organic layers were separated and the aqueous layer was extracted with Et_2O (3 × 200 mL). The organic layers were combined, dried over $MgSO_4$ and filtered. Solvent removal under reduced pressure at 0 °C afforded a dark red liquid which was subsequently purified *via* flash chromatography (20 : 1; pentanes : Et_2O) to afford after solvent removal 6.29 g (yield: 65%) of the desired product as a yellow liquid. ^{1}H NMR ($CDCl_3$, 500 MHz, ppm) δ 8.71 (1H, d), 7.38 (1H, s), 7.33 (1H), 2.92 (2H, q), 1.35 (3H, t). ^{13}C NMR ($CDCl_3$, 126 MHz, ppm) δ 165.19, 150.27, 138.77 (q), 123.09 (q), 117.83 (q), 116.72 (q), 31.58, 13.75. ^{19}F NMR ($CDCl_3$, 470 MHz, ppm) δ −64.84. ESI-MS *m*/*z* calc. for $[C_8H_8F_3N + H]^+$ 176.0687, found 176.0667.

bpy2PYMe-CF$_3$. The precursor molecule 1-(2-(4-trifluoromethyl)-pyridyl)-1-(6-2,2′-bipyridyl)ethane was synthesized as follows. A solution of freshly prepared LDA (from diisopropylamine (2.70 mL, 19.0 mmol) and butyllithium (2.5 M in hexanes, 7.66 mL, 19.0 mmol)) in THF (30 mL) was added to a solution of 2-ethyl-4-trifluoromethylpyridine (3.35 g, 19.0 mmol) in THF (80 mL) at −78 °C, which resulted in a color change to dark purple. Stirring was continued at −78 °C for 1 h, after

which a solution of 6-bromo-2,2′-bipyridine (3.00 g, 12.8 mmol) in THF (40 mL) was added, resulting in a color change to dark red. The mixture was allowed to warm to room temperature and stirred for 20 h, after which it was quenched with H_2O (50 mL) and extracted with CH_2Cl_2 (3 × 100 mL). After drying the combined organic phases over $MgSO_4$, the solvent was removed under reduced pressure and the product was purified by distillation (180 °C, 200 mTorr). Yield: 3.34 g (53%). ^{1}H-NMR ($CDCl_3$, 500 MHz, ppm): δ 8.68 (1H, d), 8.62 (1H,d), 8.40 (1H, d), 8.25 (1H, d), 7.72 (3H, m), 7.30 (1H, d), 7.26 (1H, d), 7.21 (1H, t). ^{13}C-NMR ($CDCl_3$, 126 MHz, ppm): δ 165.7, 161.9, 156.2, 155.4, 149.9, 148.9, 138.4 (q), 137.5, 136.7, 123.6, 122.9 (q), 122.4, 121.1, 118.9, 118.3 (q), 117.0 (q), 49.9, 20.1.

The synthesis of **bpy2PYMe-CF$_3$** then proceeded as follows. A solution of freshly prepared LDA (from diisopropylamine (737 μL, 5.22 mmol) and butyllithium (2.5 M in hexanes, 2.10 mL, 5.22 mmol)) in THF (30 mL) was added to a solution of 1-(2-(4-trifluoromethyl)-pyridyl)-1-(6-2,2′-bipyridyl)ethane (1.72 g, 5.22 mmol) in THF (50 mL) at −78 °C, and the resulting dark red mixture was stirred at −78 °C for 1 h. After addition of a solution of 6-bromo-2,2′-bipyridine (1.02 g, 4.35 mmol) in THF (40 mL), the mixture was allowed to warm to room temperature, stirred for 20 h and subsequently stirred at reflux for 28 h. After cooling to room temperature, quenching with 1 M $NaHCO_3$ (aq) solution (60 mL), extraction into CH_2Cl_2 (4 × 100 mL), and drying of the combined organic phases, the solvents were removed under reduced pressure. Purification by column chromatography (silica, 6 : 1 hexanes : EtOAc/1% NEt_3) yielded 1.58 g (75% yield) of pure **bpy2PYMe-CF$_3$**. Anal. calcd for $C_{28}H_{21}F_3N_5$: C, 69.56%; H, 4.17%; N, 14.49%. Found: C, 69.08%; H, 4.06%; N, 14.10%. ^{1}H-NMR ($CDCl_3$, 500 MHz, ppm): δ 8.78 (1H, d), 8.65 (2H, d), 8.31 (2H, d), 8.12 (2H, d), 7.78 (2H, t), 7.69 (2H, t), 7.64 (1H, s), 7.40 (1H, d), 7.26 (4H, m), 2.49 (3H, s). ^{13}C-NMR ($CDCl_3$, 126 MHz, ppm): δ 167.8, 164.4, 156.2, 154.7, 149.1, 148.9, 137.3 (q), 137.2, 136.8, 123.6, 123.3, 123.1 (q), 121.1, 120.6 (q), 118.5, 116.6 (q), 60.5, 27.0. IR (neat, cm^{-1}): 1579 (s), 1560 (s), 1474 (m), 1453 (s), 1426 (s), 1391 (s), 1329 (*vs.*), 1287 (vw), 1260 (w), 1205 (w), 1167 (s), 1130 (*vs.*), 1086 (s), 1067 (m), 1042 (m), 990 (m), 893 (w), 842 (m), 826 (m), 781(s), 764 (s), 748 (s), 706 (m), 675 (m), 664 (s), 638 (m), 619 (s), 584 (vw), 546 (w), 480 (w), 461 (w).

Generalized preparation for the compounds [Fe(bpy2PYMe)(CH$_3$CN)](CF$_3$SO$_3$)$_2$ (1), [Co(bpy2PYMe)(CF$_3$SO$_3$)](CF$_3$SO$_3$) (2), [Ni(bpy2PYMe)(CH$_3$CN)](BF$_4$)$_2$ (3), [Cu(bpy2PYMe)(CF$_3$SO$_3$)](CF$_3$SO$_3$) (4), and [Co(bpy2PYMe-CF$_3$)(CF$_3$SO$_3$)](CF$_3$SO$_3$) (6). Using a N_2 filled glove box, CH_3CN (14 mL) was added to a solid equimolar mixture of the corresponding metal salt and ligand (**1**: $Fe(CF_3SO_3)_2$ (170 mg, 0.480 mmol) and **bpy2PYMe** (200 mg, 0.481 mmol); **2**: $Co(CF_3SO_3)_2$ (171 mg, 0.479 mmol) and **bpy2PYMe** (200 mg, 0.481 mmol); **3**: $Ni(BF_4)_2$ (112 mg, 0.482 mmol) and **bpy2PYMe** (200 mg, 0.481 mmol); **4**: $Cu(CF_3SO_3)_2$ (90.0 mg, 0.249 mmol) and **bpy2PYMe** (104 mg, 0.250 mmol); **6**: $Co(CF_3SO_3)_2$ (148 mg, 0.414 mmol) and **bpy2PYMe-CF$_3$** (201 mg, 0.415 mmol)) and the suspension was stirred at room temperature for 20 h. Filtration through Celite and removal of solvent under reduced pressure afforded solid material of the desired metal complexes, which were subsequently recrystallized from either CH_3CN/Et_2O solvent mixtures (for **1**, **2**, **3**, and **4**) or a toluene/CH_3CN/hexanes mixture (for **6**). Crystalline yields: **1**: 303 mg (78%); **2**: 318 mg (86%); **3**: 180 mg (54%); **4**: 108 mg (56%); **6**: 265 mg (76%).

[Zn(bpy2PYMe)(CF$_3$SO$_3$)](CF$_3$SO$_3$) (5). Acetonitrile (10 mL) was added to a solid mixture of $ZnCl_2$ (19.5 mg, 0.143 mmol) and **bpy2PYMe** (59.6 mg, 0.143 mmol) and the mixture stirred for 4 h, after which $AgCF_3SO_3$ (73.7 mg, 0.287 mmol) was added. Subsequent filtration and Et_2O diffusion yielded 57 mg of crystalline **5** (Yield: 52%).

1. Anal. calcd for $C_{31}H_{24}F_6FeN_6O_6S_2$ (**1**·CH_3CN): C, 45.94%; H, 2.98%; N, 10.37%. Found: C, 45.98%; H, 3.14%; N, 10.19%. IR (neat, cm^{-1}): 1602 (m), 1471 (m), 1451 (m), 1408 (m), 1395 (m), 1249 (s), 1224 (s), 1143 (s), 1027 (s), 863 (w), 819 (m), 793 (m), 771 (s), 731 (m), 705 (w), 674 (w), 661 (w), 634 (s), 572 (m), 515 (s), 490 (w), 467 (w). ESI-MS (*m*/*z*, amu): 661.09 [M + CF_3SO_3]$^+$, 256.08 [M]$^{2+}$. ^{1}H-NMR (CD_3CN, 500 MHz, 243 K, ppm): δ 9.61 (1H, d), 9.20 (1H, d), 8.65 (1H, d), 8.38 (2H, m), 8.33 (1H, d), 8.26 (1H, t), 8.22 (1H, d), 8.11 (1H, d), 8.03 (2H, m), 7.92 (3H, m), 7.82 (1H, d), 7.28 (1H, t), 7.21 (1H, t), 6.21 (1H, d), 2.78 (3H, s). ^{13}C-NMR (CD_3CN, 126 MHz, 243 K, ppm): δ 160.0, 159.7, 159.1, 158.1, 157.3, 155.5, 155.2, 151.8, 137.8, 137.2, 137.1, 136.9, 136.7, 132.6, 125.7, 123.7, 122.7, 121.7, 120.9, 120.7, 120.1, 119.6, 119.3, 118.2, 54.9, 17.2.

2. Anal. calcd for $C_{29}H_{21}CoF_6N_5O_6S_2$ (**2**): C, 45.09%; H, 2.74%; N, 9.07%. Found: C, 45.42%; H, 3.04%; N, 9.28%. IR (neat, cm^{-1}): 1595 (m), 1579 (m), 1562 (w), 1484 (w), 1472 (w), 1451 (m), 1433 (w), 1416 (w), 1398 (w), 1299 (m), 1258 (s), 1231 (s), 1209 (s), 1173 (s), 1149 (s), 1073 (m), 1057 (m), 1029 (s), 1018 (s), 882 (w), 869 (m), 825 (m), 798 (m), 770 (s), 755 (m), 740 (w), 702 (w), 674 (m), 658 (m), 620 (*vs.*) 572 (m), 516 (s). ESI-MS (*m*/*z*, amu): 623.06 [M]$^+$. RT − χT_M = 3.2 emu kmol^{-1} corresponding to $S = 3/2$ with $g \sim 2.4$.

3. Anal. calcd for $C_{29}H_{24}B_2F_8N_6Ni$ (**3**): C, 50.56%; H, 3.51%; N, 12.20%. Found: C, 50.81%; H, 3.60%; N, 11.89%. IR (neat, cm^{-1}): 1595 (m), 1584 (m), 1567 (w), 1485 (w), 1452 (m), 1435 (m), 1382 (w), 1325 (w), 1285 (w), 1255 (w), 1171 (w), 1053 (*vs.*, br), 1023 (*vs.*), 969 (s), 917 (m), 860 (m), 822 (m), 795 (m), 772 (s), 675 (m), 664 (m), 646 (m), 575 (w), 520 (m) 492 (w). ESI-MS (*m*/*z*, amu): 257.07 [M]$^{2+}$. Paramagnetic ($S = 1$).

4. Anal. calcd for $C_{32}H_{25.5}CuF_6N_{6.5}O_6S_2$ (**4**·1.5CH_3CN): C, 45.82%; H, 3.06%; N, 10.85%. Found: C, 45.98%; H, 3.08%; N, 10.88%. IR (neat, cm^{-1}): 1606 (m), 1594 (m), 1582 (m), 1489 (w), 1453 (m), 1437 (w), 1419 (w), 1250 (*vs.*), 1222 (s) 1149 (s), 1068 (m), 1027 (s), 920 (w), 882 (w), 866 (m), 826 (w), 797 (m), 774 (s), 704 (w), 675 (m), 663 (m), 618 (*vs.*), 573 (s), 514 (s), 468 (w). ESI-MS (*m*/*z*, amu): 627.06 [M]$^+$. See Fig. S6† for the room temperature EPR spectrum of **4** in CH_2Cl_2 solution.

5. Anal. calcd for $C_{29}H_{21}ZnF_6N_5O_6S_2$ (**5**): C, 44.71%; H, 2.72%; N, 8.99%. Found: C, 45.12%; H, 3.16, N 9.35. IR (neat, cm^{-1}): 1594 (m), 1581 (m), 1566 (w), 1483 (w), 1472 (w), 1451 (m), 1432 (w), 1397 (w), 1298 (s), 1258 (s), 1232 (s), 1210 (s), 1147 (s), 1073 (m), 1056 (w), 1029 (s), 1018 (s), 882 (w), 868 (w), 825 (w), 798 (m), 770 (s), 755 (m), 740 (w), 702 (w), 674 (m), 658 (m), 634 (s), 572 (m), 516 (s). ESI-MS (*m*/*z*, amu): 628.05 [M]$^+$. ^{1}H-NMR (CD_3CN, 500 MHz, 243 K, ppm): δ 9.05 (1H, d), 8.82 (2H, d), 8.48 (2H, d), 8.38 (2H, d), 8.31 (2H, t), 8.24 (2H, t), 8.14 (2H, d), 8.05 (2H, m), 7.85 (2H, t), 7.54 (1H, t), 2.77 (3H, s). ^{13}C-NMR (CD_3CN, 125 MHz, 243 K, ppm): δ 157.2, 156.9, 149.5, 148.9,

148.8, 148.6, 142.4, 141.8, 140.7, 127.4, 124.4, 124.3, 123.4, 122.9, 122.1, 120.7, 119.5, 49.3, 21.6.

6. Anal. calcd for $C_{30}H_{20}CoF_9N_5O_6S_2$ (**6**): C, 42.87%; H, 2.40%; N, 8.33%. Found: C, 42.92%; H, 2.46%; N, 8.31%. IR (neat, cm^{-1}): 1624 (w), 1596 (m), 1582 (m), 1564 (m), 1484 (m), 1452 (m), 1408 (m), 1334 (s), 1308 (s), 1285 (s), 1263 (s), 1232 (s), 1206 (s), 1164 (s), 1144 (*vs.*), 1112 (s), 1103 (s), 1071 (m), 1025 (*vs.*), 904 (m), 883 (m), 840 (m), 819 (w), 789 (m), 767 (s), 753 (m), 706 (m), 676 (s), 643 (*vs.*), 571 (m), 515 (s) 460 (m). ESI-MS (*m*/*z*, amu): 691.05 $[M]^+$.

Crystal structure determinations

Data collection was performed on single crystals coated with Paratone-N oil and mounted on Kaptan loops. The crystals were frozen under a stream of N_2 (100 K; Oxford Cryostream 700) during measurements. Data were collected using a Bruker APEX II QUAZAR diffractometer equipped with a Microfocus Sealed Source (Incoatec IμS; Mo-Kα λ = 0.71073 Å) and APEX-II detector. Raw data were integrated and corrected for Lorentz and polarization effects using Bruker APEX2 v. 2009.1.[24] Absorption corrections were applied using SADABS.[25] Space group assignments were determined by examination of systematic absences, E-statistics, and successive refinement of the structures. Structures were solved using direct methods (**1**, **2**, **3**, **5**, and **6**) or the Patterson method (**4**) and refined by least-squares refinement on F^2 followed by difference Fourier synthesis.[26] All hydrogen atoms were included in the final structure factor calculation at idealized positions and were allowed to ride on the neighboring atoms with relative isotropic displacement coefficients. Thermal parameters were refined anisotropically for all non-hydrogen atoms. Although **1** crystallizes readily from CH_3CN/Et_2O solvent mixtures, the thus obtained crystals were repeatedly of low quality. Attempts to obtain high quality single crystal diffraction data, including crystallization in the presence of alternative counterions and at low temperatures and performing data collection at various temperatures were unsuccessful. However, the connectivity of the Fe complex (**1**) and preferred coordination of CH_3CN over $SO_3CF_3^-$ could be established unambiguously. Crystallization of **3** was only successful in the presence of NBu_4PF_6 from CH_3CN/Et_2O mixtures. Its crystal structure shows one PF_6^- disordered with a BF_4^- ion in a 1/1 ratio. The Et_2O solvent molecule is also disordered over two positions. Compound **4** crystallized with one of the triflate ion disordered over two positions with equal occupancies.

Computational methods

Density functional theory (DFT) calculations were run with the Q-Chem[27] package using the B3PW91 hybrid functional.[28] A larger than standard quadrature grid (SG-1)[29] of 75 radial points and 302 Lebedev angular points was used to ensure high-quality results. Unrestricted SCF calculations were performed using the Direct Inversion in the Iterative Subspace (DIIS) algorithm[30] with a threshold of 10^{-14} Hartrees and a convergence of 10^{-9} Hartrees. The Wachters+f basis set[31] was used for Co while the triple-ζ polarized 6-311G* basis set[32] was employed for H, C, N, F, and S. In addition, due to the ionic character of the Co–O bond, O was described with a diffuse triple-ζ polarized 6-311+G* basis set. All stationary points were fully characterized *via* analytical frequency calculations to ensure that geometries corresponded to local minima (no negative eigenvalues). Stability analyses were also performed. Single-point calculations including solvent-corrected energies have been computed *via* the SWIG C-PCM approach[33] (acetonitrile, ε = 35.688) at standard conditions (T = 298.15 K, P = 1 atm) using the UFF radii.

Photocatalysis experiments

H_2 production measurements were performed using a custom-built 16-well combinatorial apparatus. Typically, 10 mL of total catalytic solution volume prepared in a 40 mL air-tight EPA vial (VWR Scientific) was irradiated from the bottom using a royal-blue LED (Philips, Luxeon Rebel series) mounted on a starboard (LXMS-PR01-0425-CT) whose output was passed through a Fraen narrow beam lens (12° beam angle, FLP-N4-RE-HRF). The current passing through the LED was controlled by a custom-built circuit board and could be adjusted between 450 and 800 mA. The optical power output at λ_{max} = 452 ± 10 nm was monitored using a power meter and this output (typically 540 mW @ 700 mA) was fine-tuned before each run. All experiments were performed at a constant rotation speed of 150 rpm controlled by an IKA orbital shaker. All reaction vials and LEDs were temperature controlled (20 °C) by aluminum blocks cooled using a circulating chiller. Solutions containing ascorbic acid/ascorbate (H_2A/HA^-) (prepared by titration of ascorbic acid with NaOH) and the photosensitizer were thoroughly deaerated using a number of vacuum/argon pressurization cycles. The molecular cobalt catalysts were introduced under inert atmosphere and degassing was continued, and ultimately terminated by equilibration to atmospheric pressure. The vials were each connected to pressure transducers (SSI technologies, P51 pressure sensors) through a Teflon spacer using stainless steel fittings and separately to a universal gas analyzer (Stanford Research Systems, UGA-hydrogen) through capillary tubes. During the course of a given reaction, head space pressure was monitored in real-time using a multifunction data acquisition box (National Instruments, NI-USB-6210) and data were logged using LabVIEW SignalExpress software. After the end of each photocatalytic reaction, headspace sampling (100 μL) was performed using a Hamilton syringe followed by injection into a GC-8A (Shimadzu) equipped with a 5 Å molecular sieves column and TCD operated with argon carrier gas. During the course of the various photocatalysis reactions, the headspace was pressurized from H_2 buildup and this was equilibrated to atmospheric pressure before the percent H_2 measured relative to argon was analyzed by mass spectroscopy. GC and MS data were calibrated against a certified Ar/H_2 standard (Praxair). Quantitative results of H_2 evolution were typically averaged and the processed pressure data were normalized to the final amounts of H_2 obtained.

The quantum yield values have been deduced from the rates of hydrogen production (Fig. 5, top) using the LED output

(452 ± 10 nm, 540 mW) with an experimental error of ~10%. These quantum yields are based on two photons absorbed (eqn (1)).

$$\Phi = \frac{2 \times n_{H_2}}{n_{photons}} \quad (1)$$

Where n_{H_2} is the number of hydrogen produced as measured in the headspace of the reactors, and $n_{photons}$ is the number of photons absorbed by the samples as calculated from eqn (2).

$$n_{photons} = \frac{P_{abs} \times t}{E_{photons} \times N_a} \quad (2)$$

Where P_{abs} is the optical power (W) absorbed by the sample which is equal to the output photon flow of the LED measured after the focusing lens (540 mW) given that the transmittance of the solution (2 cm pathlength) is negligible at the concentration utilized in Fig. 5 top; t is the irradiation time in (s), E_{photon} is the energy of a photon (J) assuming monochromatic light, and N_a is Avogadro's number. This method of calculating the quantum yield has been utilized by Bernhard and coworkers on a setup similar to the one described above.[34]

Photoluminescence quenching

Optically dilute samples (O.D. = 0.1–0.3 at λ_{exc} = 452 nm) were placed in 1 cm pathlength cuvettes and deaerated by ~1 h Ar bubbling and then kept under positive pressure of Ar during the course of the experiments. Data were collected with an Edinburgh Instruments laser flash photolysis system (LP920) equipped with LP900 software. The excitation source was a Vibrant LD 355 II Nd:YAG/OPO system (OPOTEK), (~5 mJ per pulse, 1 Hz). Kinetic traces at a specific wavelength were acquired using a PMT (R928 Hamamatsu).

Results and discussion

Syntheses and structures

The pentadentate ligands **bpy2PYMe** and **bpy2PYMe-CF$_3$** were prepared in two steps starting from commercially available 6-bromo-2,2′-bipyridine and 2-ethylpyridine or 2-ethyl-4-trifluoromethylpyridine, respectively.[35] Complex formation is facile in acetonitrile using metal salts of Fe^{2+}, Co^{2+}, Ni^{2+}, Cu^{2+}, and Zn^{2+}, and diffusion of Et_2O yielded crystalline material of red **1**, green-orange **2**, pale pink **3**, blue **4**, colorless **5**, and green **6**, respectively (Scheme 3).

The solid-state structures of compounds **1–6** were established by means of single crystal X-ray diffraction (see Fig. 1 and S1–S4; crystallographic information and bond lengths are given in Tables S1 and S2†). For all six complexes, **bpy2PYMe** or **bpy2PYMe-CF$_3$** act as pentadentate ligands, leaving one coordination side of the transition metal available for exogenous ligands such as acetonitrile (**1**, **3**) or trifluoromethanesulfonate (**2**, **4**, **5**, **6**). The coordination geometry around the metal ion is strongly distorted from idealized geometries for six coordinate metal centers. Notably, binding of the metal ions to the bpy moieties is asymmetric: the inner pyridine of each bpy binds significantly closer to the metal center ($M–N_{bpy(s)}$) than the outer pyridine ($M–N_{bpy(l)}$) of the same moiety ($d(M–N_{bpy(l)}) – d(M–N_{bpy(s)}) = \sim 0.05$ Å for **1–6**). This is in stark contrast to the crystal structures of $[M(bpy)_3]^{2+}$ complexes in which the octahedral M^{2+} ion displays only minor differences in M–N bond lengths. However, similar asymmetric binding to bpy ligand moieties have been observed in closely related Co^{2+} complexes of ligand sets like PY4[3a] ($d(M–N_{bpy(l)}) – d(M–N_{bpy(s)}) = 0.055$ Å) and a hexadentate tris-bpy ligand[36] ($d(M–N_{bpy(l)}) – d(M–N_{bpy(s)})_{avg} = 0.053$ Å).

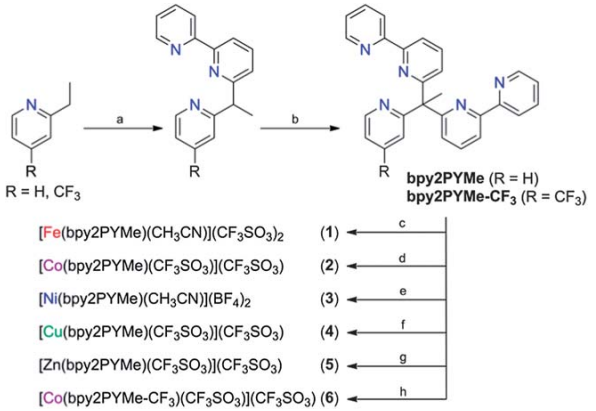

Scheme 3 Syntheses of ligands and metal complexes. [Reagents: (a) BuLi (R = H) or LDA (R = CF_3), 2-Br-bpy; (b) BuLi (R = H) or LDA (R = CF_3), 2-Br-bpy; **bpy2PYMe** complexation: (c) $Fe(CF_3SO_3)_2$; (d) $Co(CF_3SO_3)_2$; (e) $Ni(BF_4)_2$; (f) $Cu(CF_3SO_3)_2$; (g) $ZnCl_2$, 2 $Ag(CF_3SO_3)$, –2 AgCl; **bpy2PYMe-CF$_3$** complexation: (h) $Co(CF_3SO_3)_2$].

Utilizing the continuous shape measure program SHAPE2,[37] we calculated the comparative shape integrals for the octahedral (S(Oct)) and trigonal prismatic (S(TP)) cases and found that Co environment in complexes **2** and **6** can be described as closer to trigonal prismatic (S(TP) = 4.2) than octahedral (S(Oct) = 5.5) but lying along the Bailar path (with a deviation of 5.4). For the other complexes more pronounced deviations from the Bailar path were calculated. The coordination environment of Cu in **4** (Fig. S3†) is unique within this family of complexes in that the Cu^{2+} ion features a very long Cu–O distance of ~2.78(2) Å *trans* to the pyridine moiety of **bpy2PYMe**. Co complexes **2** and **6**

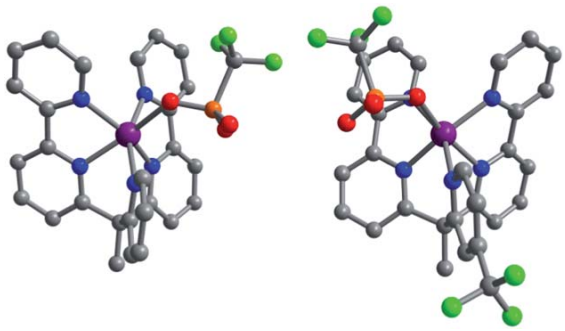

Fig. 1 Molecular structures of the monocationic Co complexes in the crystal structures of **2** (left) and **6** (right). Purple, blue, grey, red, orange, and green spheres represent Co, N, C, O, S, and F atoms, respectively; hydrogen atoms have been omitted for clarity.

display almost identical Co–N bond distances (2.071(2)–2.183(2) Å in **2**; 2.078(2)–2.198(2) Å in **6**) which are similar to those observed for the high-spin Co(II) ($S = 3/2$) ion in $[Co(PY5Me_2)(CH_3CN)]^{2+}$ (2.095(3)–2.142(3) Å).[4d]

Electrochemistry

Compounds **1–6** can undergo multiple redox changes, as evidenced by the cyclic voltammograms (CVs) in Fig. 2 (potentials are given in Table S3†).

The Fe complex of **1** displays a single reversible oxidation wave at 686 mV (*vs.* ferrocene) that we assign to the ferrous/ferric redox couple. Interestingly, **1** also shows three reversible one-electron reduction events at −1546, −1664 mV, and −2349 mV. The first two reductions appear at potentials similar to those of the two closely spaced reductions observed in the CV of the Zn(II) complex in **5** (at −1629 and −1763 mV). We therefore assign the first two reduction events for **1** as ligand centered in nature (presumably yielding a ferrous diradical complex) and the third reduction as the $Fe^{2+/1+}$ couple.

The CV of **3** features reversible $Ni^{2+/3+}$ and $Ni^{2+/1+}$ redox events at 1392 and −1199 mV, respectively. Notably, the Ni^{1+} state is more easily accessible than in the corresponding pyridine complex $[Ni(PY5Me_2)(CH_3CN)]^{2+}$ ($E_{1/2}(Ni^{2+/3+}) = 1320$ mV; $E_{1/2}(Ni^{2+/1+}) = -1610$ mV)[38] which underlines the improved ability of **bpy2PYMe** to stabilize metal ions of lower oxidation states. At more negative potentials, three additional reversible reduction events occur at −1759, −2186, and −2581 mV, which have not been further investigated but likely involve both, metal ($Ni^{1+/0}$) and ligand based reductions.

The copper complex in **4** displays a reversible $Cu^{2+/1+}$ reduction at −837 mV. Scans to more negative potentials result in plating of Cu^0 as evidenced by the stripping wave in the CV. The CV of **2** shows two closely spaced reductions at −1786 and −1941 mV, which we assign to reductions of the bpy moieties of the ligand. However, these reductions are preceded by the formal $Co^{2+/1+}$ couple at −1197 mV which is 230 mV more positive than the one observed for $[Co(CH_3CN)(PY5Me_2)]^{2+}$ and may indicate stabilization of Co^{1+} through π backbonding to bpy. The greater than 120 mV more negative reduction potentials of the bpy moieties in **2** as compared to **1** and **5** reflect the well established sensitivity of bpy reduction potentials for the charge of the M^{n+} ion ($n = 1$ for **2**; $n = 2$ for **1**, **5**).[39] Additionally, there is a broad $Co^{2+/3+}$ redox event centered at 235 mV. The broadness of this feature is common to this class of Co complexes and is likely due to the significant structural reorganization in going from high-spin Co^{2+} to a presumably low-spin Co^{3+} species.

Given the sensitivity of the Co^{2+} ion in the $PY5Me_2$ series to substitutions in 4-position of the central pyridine ligand,[4d] we also investigated the electrochemical properties of **6**, in which the ligand bears an electron-withdrawing CF_3 group in 4-position of the pyridine moiety. As expected, the CV of **6** (Fig. S5†) is qualitatively the same as that of **2**, with the $Co^{2+/3+}$ and $Co^{2+/1+}$ couples shifted positively by 75 and 61 mV, respectively. Surprisingly, the potential of the two ligand-centered reductions are shifted more positively (~80 mV) than the metal centered reduction. This unexpected observation indicates the strongly delocalized nature of the one-electron reduced Co complex, likely through π interactions between Co^{1+} and the bpy moieties.

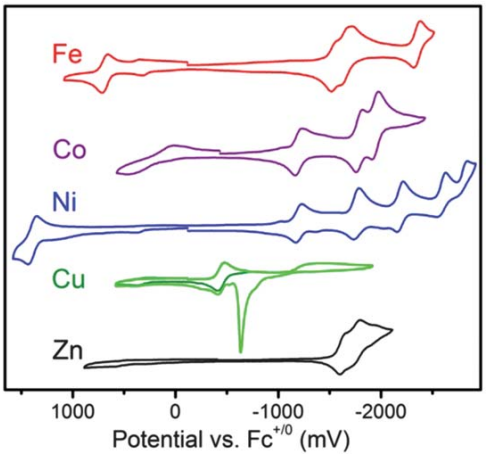

Fig. 2 Cyclic voltammograms of ~1 mM solutions of **1**, **2**, **3**, **4**, and **5** (top to bottom) measured in CH_3CN (0.1 M NBu_4PF_6, $\nu = 100$ mV s^{-1}).

Electrocatalytic studies with acetic acid in acetonitrile

Compounds **1**, **2**, **3**, and **5** were initially evaluated by cyclic voltammetry as possible electrocatalysts for the reduction of protons. The current response to addition of various amounts of acetic acid ($E^0_{CH_3CN}(CH_3CO_2H) = -1.46$ V[40a] or −1.23 V[40b] *vs.* $Fc^{+/0}$) resulted in significant current enhancement (as compared to the bare glassy carbon electrode under the same conditions) only for the Co complexes of **2** and **6**. This type of response indicates significant catalytic turnover on the timescale of the experiment. The catalytic current response to addition of aliquots of CH_3CO_2H to solutions of **2** and **6** is shown in Fig. 3 at the top and middle, respectively.

Importantly, for both compounds we observe two discrete events (E1, E2) of current enhancement at potentials that match well with the ligand reduction potentials in the absence of acid (black trace in Fig. 3). For **2**, the current at E1 is CH_3CO_2H concentration dependent up to 90 mM and scanning to even more negative potentials accesses E2, which shows even higher current densities. The evolution of hydrogen at these potentials was determined separately by means of bulk electrolysis and GC analysis of the head space (indicating ~90% Faradaic efficiency).

It thus appears that **2** may operate from two regimes with different rates, depending on the applied potential, although the increased driving force at more negative potentials and the decrease in local proton concentration after E1 biases a quantitative description. The current response in the CV of **6** to addition of CH_3CO_2H is significantly different. In particular, only a small current increase is observed at E1, which levels off at lower CH_3CO_2H concentrations, indicating much slower catalytic turnover as compared to E1 in **2**. However, significant

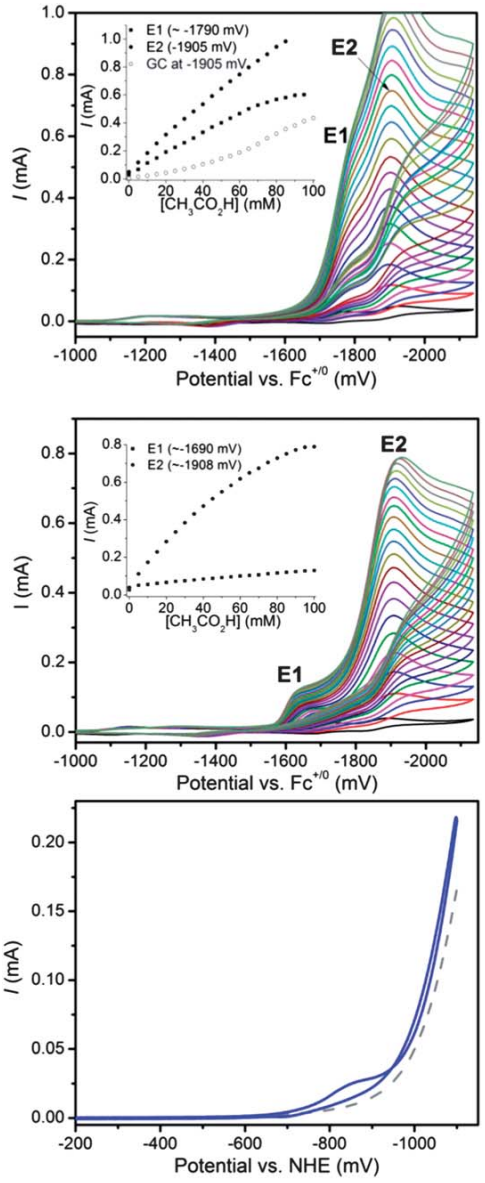

Fig. 3 Electrochemical response of 1 mM **2** (top) and **6** (middle) to addition of acetic acid (0–100 eq.) in CH_3CN (0.1 M NBu_4PF_6, ν = 100 mV s^{-1}). Insets: $[CH_3CO_2H]$ dependence of current at selected potentials. Cyclic voltammogram (ν = 100 mV s^{-1}) of 0.3 mM **2** (bottom, blue trace) in aqueous 0.3 M ascorbic acid/ascorbate at pH 4 (grey dashed trace corresponds to glassy carbon background).

current enhancement was observed for E2, albeit with overall lower current densities than in **2**. These experiments are useful *proof-of-principle* studies that emphasize the beneficial role of ligand-based redox activity for improved electrocatalytic proton reduction, while indicating the validity of the concept introduced above (blue solid trace in Scheme 1). It is noteworthy that the catalytic onset in similar experiments utilizing the Co complex of the redox-innocent ligand (CF_3-PY5Me_2) is observed at much more negative potentials (Fig. S8†) that have to involve the Co^0 state (blue dashed trace in Scheme 1). The reduced catalytic performance of **6** as compared **2** is contrary to the trend observed for Co complexes of the PY5Me_2 ligand family.

Electronic structure calculations

In an effort to explain these counterintuitive results, we employed DFT calculations to gain insight into the electronic structures of **2** and **6**. We use isodesmic reactions as previously reported by Solis and Hammes-Schiffer[5d,41] to eliminate systematic computational errors (solvation effect, basis sets, exchange and correlation functional). In this case, we found that the reduction potential from Co^{II} to Co^{I} is switched by 78 mV from R = CF_3 to R = H, which is in good agreement with the experiment ($\Delta E^{1/2}$ = 61 mV). The optimized molecular structures (Table S4†) match the experimentally determined Co geometries in **2** and **6** reasonably well, although the Co–O bond is calculated to be 0.11 and 0.06 Å shorter in **2** and **6**, respectively (it was found that the potential energy surface is relatively insensitive to small variations in Co–O bond length; see Fig. S10†).

The highly distorted geometry around the S = 3/2 Co(II) center causes a d-orbital splitting reminiscent of the trigonal prismatic case, with an electron configuration of $d_{z^2}{}^2 d_{x^2-y^2}{}^2 d_{xy}{}^1 d_{xz}{}^1 d_{yz}{}^1$ (Fig. S11†). In going from **2** to **6**, all relevant valence orbitals (and LUMOs) are lowered in energy, which is in good agreement with the observed trends in redox potentials.

Preliminary computational results on the one-electron reduced (S = 1) species of **2** (**2**+**e**$^-$) and **6** (**6**+**e**$^-$) indicate that $CF_3SO_3^-$ dissociation and CH_3CN binding to Co(I) is favored.[42] As can be seen in Fig. 4, all orbitals are energetically stabilized by the introduction of the CF_3 group, with the β-HOMO (d_{xy}) being most strongly affected. Interestingly, the percentage of metal d orbital character, as determined by a partial Lowdin population analysis, is even more significantly affected. In particular, overall higher metal character in **6**+**e**$^-$ as compared to **2**+**e**$^-$was determined with the α-HOMO-3 (d_{z^2}) and β-HOMO (d_{xy}) increasing in metal character by 13% and 3%, respectively. The metal d_{xy} orbital in this distorted C_3 symmetry features almost perfect π symmetry with respect to one of the bpy moieties. While both, experimental and theoretical work aimed at characterizing the one-, two-, and three-electron reduced species of **2** and **6** are ongoing, we may offer a tentative explanation for the observed differences in catalysis: one-electron reduction of the Co(II) complex yields a formal Co(I) species. The reduced σ donating ability of the CF_3 substituted pyridine group in **6** stabilizes the Co(I) complex and reduces the extent of π backbonding from Co to the bpy π* orbitals. This results in the observed increase in spin population on Co in **6**+**e**$^-$ as compared to **2**+**e**$^-$. Furthermore, the reduced spin character of the ligand in **6**+**e**$^-$ is in good agreement with the observed positive shift in ligand reduction potentials, as determined by cyclic voltammetry. Clearly, the introduction of the CF_3 group indirectly effects the π interactions between Co and the ligand. At E1, another electron is added into the ligand π* orbital, which disturbs the π backbonding interaction and renders the Co center in **2** sufficiently basic to react with a proton at E1. In **6**,

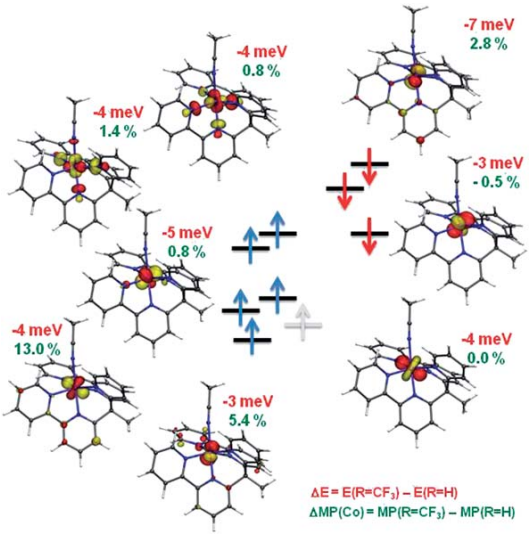

Fig. 4 Relevant one electron alpha (blue) and beta (red) valence orbitals calculated for **2+e**$^-$. The red and green values correspond to the calculated differences in energy and metal population (MP) of the orbitals upon CF_3 substitution (according to Lowdin population analysis).

however, "communication" between the π* ligand orbitals is diminished, and less catalytic activity is observed at E1.

The foregoing experiments in organic solvents offer valuable first insights into the catalytic pathways of **2** and **6**. However, the ability of an H_2 evolution catalyst to function in water is essential. Initial electrochemical evaluation of **2** in aqueous media (Fig. 3, bottom) on glassy carbon electrodes indicated initial catalyst ($Co^{2+/1+}$) reduction followed by catalytic H_2 evolution. Consequently, we comparatively evaluated the performance of **2** and **6** in aqueous media under photocatalytic conditions.

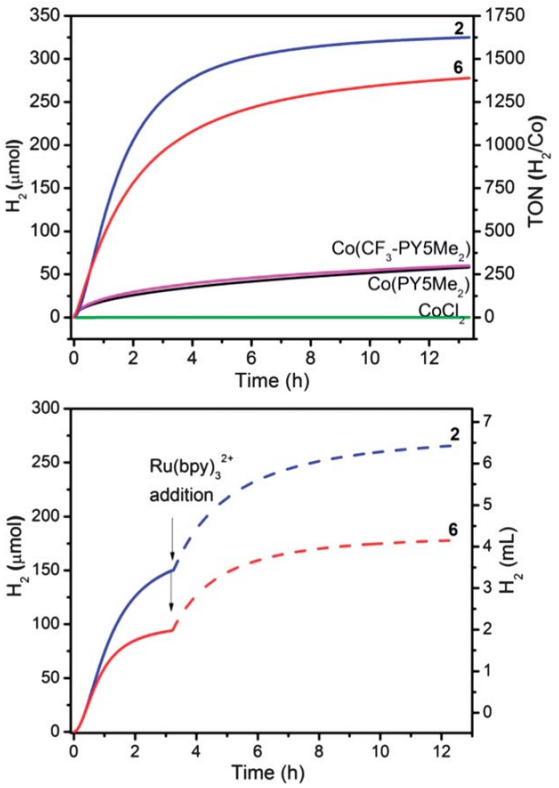

Fig. 5 Comparison of H_2 evolution during 452 ± 10 nm photocatalysis in water using 3.3×10^{-4} M $[Ru(bpy)_3]^{2+}$ and 2.0×10^{-5} M solutions of **2** (blue, pH 4), **6** (red, pH 4.5), $Co(CF_3\text{-}PY5Me_2)$ (magenta, pH 6), $Co(PY5Me_2)$ (black, pH 6) and $CoCl_2$ (green, pH 4) in the presence of 0.3 M ascorbic acid/ascorbate (top). Regeneration of catalytic activity resulting from the addition of one equivalent of $[Ru(bpy)_3]^{2+}$ in compositions containing 2.0×10^{-5} M of **2** (blue, pH 4) and **6** (red, pH 4) after 3 h of continuous illumination in the presence of 1.1×10^{-4} M $[Ru(bpy)_3]^{2+}$ initially (bottom).

Photocatalytic proton reduction in water

Photocatalytic experiments ($\lambda_{ex} = 452 \pm 10$ nm, 540 mW) were performed at optimized pH values in a custom-built combinatorial photoreactor using various cobalt catalysts at fixed concentration (2.0×10^{-5} M), with $[Ru(bpy)_3]^{2+}$ photosensitizers at 3.3×10^{-4} M and in the presence of ascorbic acid/ascorbate (Fig. 5, top) as a sacrificial reductant. Fig. S12, S16, and S17† illustrate the combinatorial searches that ultimately led to the optimized photocatalysis conditions presented in Fig. 5, top. In this apparatus, real-time H_2 evolution was monitored using pressure transducers and the molecular composition of the headspace confirmed independently using GC[43] and mass spectrometry.

Under optimized conditions, the composition with catalyst **2** produced copious amounts of H_2 with an estimated initial TOF with respect to catalyst of 660 h^{-1} (Fig. 5, top). Similar to the electrochemical studies performed in acetonitrile, catalyst **6** displays somewhat lower H_2 evolution activity, with an initial TOF of 500 h^{-1}. However, both of these **bpy2PYMe**-based molecules clearly outperform the previously reported $Co(PY5Me_2)$ and $Co(CF_3\text{-}PY5Me_2)$ catalysts in optimized side-by-side comparisons, as shown in Fig. 5. Control experiments using $CoCl_2$ as a catalyst (Fig. 5, green line), the removal of light activation, or deletion of any single molecular constituent resulted in little to no H_2 production. Furthermore, no considerable change in activity was observed if the photocatalytic experiments were performed in the presence of Hg (0.1 mL), consistent with the homogeneous nature of the reactions (Fig. S13†).[43,44] Similarly, the linear increase of hydrogen production scaling directly with both catalyst and sensitizer concentration (Fig. S14 and S15†) strongly suggests that the reactions are indeed homogeneous in nature. The H_2 evolution ceases after approximately 13 h of continuous irradiation, with catalysts **2** and **6** achieved total TONs of 1630 and 1390, respectively.

The quantum yield values (Φ) using **2** or **6** were calculated to be 3.6% and 2.7%, respectively, and compare favorably with other visible light driven homogenous HER systems.[45]

Another crucial observation relates to the noteworthy stability of **2** and **6** as decreases in the rate of hydrogen production at pH 4 in the presence of lower concentrations of $[Ru(bpy)_3]^{2+}$ (1.1×10^{-4} M) was found to be largely induced by

the decomposition of the photosensitizer. Addition of one equivalent of fresh $[Ru(bpy)_3]^{2+}$ to the respective catalytic mixtures after 3 h of irradiation largely restored the H_2 evolution activity (Fig. 5, bottom), whereas addition of fresh catalyst in parallel experiments did not. $[Ru(bpy)_3]^{2+}$ has been shown to undergo ligand loss and photoanation under irradiation.[46]

The photocatalytic hydrogen production is initiated by an initial electron transfer from ascorbate (HA^-) to $*[Ru(bpy)_3]^{2+}$ ($\tau = 0.6$ μs) to produce the $[Ru(bpy)_3]^{+}$ and the ascorbate radical (HA˙).[19c] The reductive quenching rate constant is 2.6×10^7 M^{-1} s^{-1} at pH 4 (Fig. S18 and S19†). Note that $*[Ru(bpy)_3]^{2+}$ is not oxidatively quenched by the Co(II) catalysts at the concentrations used in our photocatalytic experiments. However, $[Ru(bpy)_3]^{+}$ possesses a redox potential (−1.26 V *vs.* NHE[47]) sufficiently negative to allow for electron transfer to both, the Co(II) and Co(I) species of **2** as estimated from the electrochemical analysis described above.

Conclusions

The Co complex in **2** displays dramatically improved performance for both electrocatalytic and photocatalytic generation of H_2 as compared to the earlier reported Co catalysts of the redox-inert $PY5Me_2$ family. The introduction of an electron-withdrawing CF_3 group into the pyridine moiety of the ligand in **6** was shown to have a negative impact on the catalytic performance for both electrocatalytic proton reduction in acetonitrile and photocatalytic proton reduction in aqueous media. Based on DFT results, we suggest that the π back bonding interactions between Co(I) and the π* ligand orbitals are reduced in **6**, because the Co(I) species is too strongly stabilized. This study exemplifies the beneficial interplay of metal- and ligand-centered redox activity for proton reduction catalysis and its sensitivity to ligand substitutions.

Acknowledgements

Catalyst development and characterization and DFT calculations are based upon work performed at the Joint Center for Artificial Photosynthesis, a DOE Innovation Hub, supported through the Office of Science of the U.S. Department of Energy under Award Number DE-SC0004993. Photocatalytic experiments were carried out at BGSU under support from the National Science Foundation (CHE-1012487). Prof. Stefan Bernhard is acknowledged for his assistance with the combinatorial photoreactor design. C.J.C. is an Investigator with the Howard Hughes Medical Institute and his contributions were supported by DOE/LBL grant 403801. R.S.K. was funded by a McMaster fellowship. D.Z.Z. thanks the National Science Foundation for a predoctoral fellowship.

Notes and references

1 A. W. Maverick and H. B. Gray, *Science*, 1981, **214**, 1201; N. S. Lewis and D. G. Nocera, *Proc. Natl. Acad. Sci. U. S. A.*, 2006, **103**, 15729; J. J. Concepcion, R. L. House, J. M. Papanikolas and T. J. Meyer, *Proc. Natl. Acad. Sci. U. S. A.*, 2012, **109**, 15560.

2 M. R. Dubois and D. L. Dubois, *Acc. Chem. Res.*, 2009, **42**, 1974; V. Artero, M. Chavarot-Kerlidou and M. Fontecave, *Angew. Chem., Int. Ed.*, 2011, **50**, 7238; *Angew. Chem.*, 2011, **123**, 7376; P. Du and R. Eisenberg, *Energy Environ. Sci.*, 2012, **5**, 6012; M. Wang, L. Chen and L. Sun, *Energy Environ. Sci.*, 2012, **5**, 6763.

3 (*a*) J. P. Bigi, T. E. Hanna, W. H. Harman, A. Chang and C. J. Chang, *Chem. Commun.*, 2010, **46**, 958; (*b*) M. L. Helm, M. P. Stewart, R. M. Bullock, M. R. DuBois and D. L. DuBois, *Science*, 2011, **333**, 863; (*c*) V. S. Thoi, H. I. Karunadasa, Y. Surendranath, J. R. Long and C. J. Chang, *Energy Environ. Sci.*, 2012, **5**, 7762; (*d*) M. J. Rose, H. B. Gray and J. R. Winkler, *J. Am. Chem. Soc.*, 2012, **134**, 8310.

4 (*a*) H. I. Karunadasa, C. J. Chang and J. R. Long, *Nature*, 2010, **464**, 1329; (*b*) L. A. Berben and J. C. Peters, *Chem. Commun.*, 2010, 398; (*c*) C. C. L. McCrory, C. Uyeda and J. C. Peters, *J. Am. Chem. Soc.*, 2012, **134**, 3164; (*d*) Y. Sun, J. P. Bigi, N. A. Piro, M. L. Tang, J. R. Long and C. J. Chang, *J. Am. Chem. Soc.*, 2011, **133**, 9212; (*e*) H. I. Karunadasa, E. Montalvo, Y. Sun, M. Majda, J. R. Long and C. J. Chang, *Science*, 2012, **335**, 698; (*f*) V. S. Thoi, Y. Sun, J. R. Long and C. J. Chang, *Chem. Soc. Rev.*, 2013, **42**, 2388.

5 (*a*) A. D. Wilson, R. H. Newell, M. J. McNevin, J. T. Muckerman, M. R. DuBois and D. L. DuBois, *J. Am. Chem. Soc.*, 2006, **128**, 358; (*b*) J. L. Dempsey, B. S. Brunschwig, J. R. Winkler and H. B. Gray, *Acc. Chem. Res.*, 2009, **42**, 1995; (*c*) J. L. Dempsey, J. R. Winkler and H. B. Gray, *J. Am. Chem. Soc.*, 2010, **132**, 16774; (*d*) B. H. Solis and S. Hammes-Schiffer, *Inorg. Chem.*, 2011, **50**, 11252; (*e*) U. J. Kilgore, J. A. S. Roberts, D. H. Pool, A. M. Appel, M. P. Stewart, M. Rakowski DuBois, W. G. Dougherty, W. S. Kassel, R. M. Bullock and D. L. DuBois, *J. Am. Chem. Soc.*, 2011, **133**, 5861; (*f*) M. Dupuis, S. Chen, S. Raugei, D. L. DuBois and R. M. Bullock, *J. Phys. Chem. A*, 2011, **115**, 4861; (*g*) A. E. King, Y. Surendranath, N. A. Piro, J. P. Bigi, J. R. Long and C. J. Chang, *Chem. Sci.*, 2013, **4**, 1578.

6 J. A. S. Roberts and R. M. Bullock, *Inorg. Chem.*, 2013, **52**, 3823.

7 P. Chaudhuri, M. Hess, T. Weyhermüller and K. Wieghardt, *Angew. Chem., Int. Ed.*, 1999, **38**, 1095; M. Königsmann, N. Donati, D. Stein, H. Schonberg, J. Harmer, A. Sreekanth and H. Grutzmacher, *Angew. Chem.*, 2007, **119**, 3637; *Angew. Chem., Int. Ed.*, 2007, **46**, 3567; M. R. Ringenberg, S. L. Kokatam, Z. M. Heiden and T. B. Rauchfuss, *J. Am. Chem. Soc.*, 2008, **130**, 788; A. L. Smith, K. I. Hardcastle and J. D. Soper, *Inorg. Chem.*, 2010, **50**, 9864; P. J. Chirik and K. Wieghardt, *Science*, 2010, **327**, 794; A. L. Smith, K. I. Hardcastle and J. D. Soper, *J. Am. Chem. Soc.*, 2010, **132**, 14358; T. Marshall-Roth, S. C. Liebscher, K. Rickert, N. J. Seewald, A. G. Oliver and S. N. Brown, *Chem. Commun.*, 2012, **48**, 7826; J. M. Hoyt, K. T. Sylvester, S. P. Semproni and P. J. Chirik, *J. Am. Chem. Soc.*, 2013, **135**, 4862.

8 R. M. Kellett and T. G. Spiro, *Inorg. Chem.*, 1985, **24**, 2373; I. Bhugun, D. Lexa and J.-M. Saveant, *J. Am. Chem. Soc.*, 1996, **118**, 3982.
9 F. Zhao, J. Zhang, T. Abe, D. Wohrle and M. Kaneko, *J. Mol. Catal. A: Chem.*, 1999, 245.
10 D. Sellman, M. Ceck and M. Moll, *J. Am. Chem. Soc.*, 1991, **113**, 5259.
11 W. R. McNamara, Z. Han, P. J. Alperin, W. W. Brennessel, P. L. Holland and R. Eisenberg, *J. Am. Chem. Soc.*, 2011, **133**, 15368.
12 O. R. Luca, S. J. Konezny, J. D. Blakemore, D. M. Colosi, S. Saha, G. W. Brudvig, V. S. Batista and R. H. Crabtree, *New J. Chem.*, 2012, **36**, 1149. For a recent review of redox active ligands in catalysis see: O. R. Luca and R. H. Crabtree, *Chem. Soc. Rev.*, 2013, **42**, 1440.
13 L. L. Efros, H. H. Thorp, G. W. Brudvig and R. H. Crabtree, *Inorg. Chem.*, 1992, **31**, 1722.
14 B. D. Stubbert, J. C. Peters and H. B. Gray, *J. Am. Chem. Soc.*, 2011, **133**, 18070.
15 P. Connolly and J. H. Espenson, *Inorg. Chem.*, 1986, **25**, 2684; M. Razavet, V. Artero and M. Fontecave, *Inorg. Chem.*, 2005, **44**, 4786; X. Hu, B. M. Cossairt, B. S. Brunschwig, N. S. Lewis and J. C. Peters, *Chem. Commun.*, 2005, 4723; C. Baffert, V. Artero and M. Fontecave, *Inorg. Chem.*, 2007, **46**, 1817; X. Hu, B. S. Brunschwig and J. C. Peters, *J. Am. Chem. Soc.*, 2007, **129**, 8988.
16 O. Pantani, S. Naskar, R. Guillot, P. Millet, E. Anxolabehére-Mallart and A. Aukauloo, *Angew. Chem., Int. Ed.*, 2008, **120**, 9948; P. Millet, N. Mbemba, S. A. Grigoriev, V. N. Fateev, A. Aukauloo and C. Etievant, *Int. J. Hydrogen Energy*, 2011, **36**, 4134; Y. Z. Voloshin, A. V. Dolganov, O. A. Varzatskii and Y. N. Bubnov, *Chem. Commun.*, 2011, **47**, 7737.
17 L. I. Simandi, Z. Szeverenyi and E. Budo-Zahonyi, *Inorg. Nucl. Chem. Lett.*, 1975, **11**, 773; M. Kirch, J.-M. Lehn and J.-P. Sauvage, *Helv. Chim. Acta*, 1979, **62**, 1345; E. Anxolabehere-Mallart, C. Costentin, M. Fournier, S. Nowak, M. Robert and J.-M. Saveant, *J. Am. Chem. Soc.*, 2012, **134**, 6104.
18 T. Saji and S. J. Aoyagui, *J. Electroanal. Chem. Interfacial Electrochem.*, 1974, **60**, 1; Y. Kaizu, Y. Torii and H. Kobayashi, *Bull. Chem. Soc. Jpn.*, 1970, **43**, 3296; G. M. Waind and B. Martin, *J. Inorg. Nucl. Chem.*, 1958, **8**, 551; B. S. Brunschwig, C. Creutz, D. H. Macartney, T.-K. Sham and N. Sutin, *Faraday Discuss. R. Soc. Chem.*, 1982, **74**, 113; D. J. Szalda, C. Creutz, D. Mahajan and N. Sutin, *Inorg. Chem.*, 1983, **22**, 2372; D. K. Lavallee, M. D. Baughman and M. P. Phillips, *J. Am. Chem. Soc.*, 1977, **99**, 718; R. J. Fitzgerald, B. B. Hutchinson and K. Nakamoto, *Inorg. Chem.*, 1970, **9**, 2618.
19 (*a*) C. V. Krishnan, B. S. Brunschwig, C. Creutz and N. Sutin, *J. Am. Chem. Soc.*, 1985, **107**, 2005; (*b*) C. V. Krishnan, C. Creutz, D. Mahajan, A. H. Schwarz and N. Sutin, *Isr. J. Chem.*, 1982, **22**, 98; (*c*) C. V. Krishnan and N. Sutin, *J. Am. Chem. Soc.*, 1981, **103**, 2141.
20 J. Dong, M. Wang, P. Zhang, S. Yang, J. Liu, X. Li and L. Sun, *J. Phys. Chem. C*, 2011, **115**, 15089; J. I. Goldsmith, W. R. Hudson, M. S. Lowry, T. H. Anderson and S. Bernhard, *J. Am. Chem. Soc.*, 2005, **127**, 7502; S. Jasimuddin, T. Yamada, K. Fukuju, J. Otsuki and K. Sakai, *Chem. Commun.*, 2010, **46**, 8466.
21 G. M. Brown, B. S. Brunschwig, C. Creutz, J. F. Endicott and N. Sutin, *J. Am. Chem. Soc.*, 1979, **101**, 1298; W. R. McNamara, Z. Han, C.-J. Yin, W. W. Brennessel, P. L. Holland and R. Eisenberg, *Proc. Natl. Acad. Sci. U. S. A.*, 2012, **109**, 15594; M. Guttentag, A. Rodenberg, C. Bachmann, A. Senn, P. Hamm and R. Alberto, *Dalton Trans.*, 2012, **42**, 334.
22 W. M. Singh, T. Baine, S. Kudo, S. Tian, X. A. N. Ma, H. Zhou, N. J. DeYonker, T. C. Pham, J. C. Bollinger, D. L. Baker, B. Yan, C. E. Webster and X. Zhao, *Angew. Chem., Int. Ed.*, 2012, **124**, 6043; C. Bachmann, M. Guttentag, B. Spingler and R. Alberto, *Inorg. Chem.*, 2013, **52**, 6055; M. Guttentag, A. Rodenberg, C. Bachmann, A. Senn, P. Hamm and R. Alberto, *Dalton Trans.*, 2013, **42**, 334.
23 P. Du, J. Schneider, G. Luo, W. W. Brennessel and R. Eisenberg, *Inorg. Chem.*, 2009, **48**, 4952.
24 APEX2, v. 2009, *Bruker Analytical X-Ray Systems, Inc*, Madison, WI, 2009.
25 G. M. Sheldrick, *SADABS, Version 2.03; Bruker Analytical X-ray Systems, Inc*, Madison, WI, 2000.
26 O. V. Dolomanov, L. J. Bourhis, R. J. Gildea, J. A. K. Howard and H. Puschmann, *J. Appl. Crystallogr.*, 2009, **42**, 339.
27 Y. Shao, L. F. Molnar, Y. Jung, J. Kussmann, C. Ochsenfeld, S. T. Brown, A. T. B. Gilbert, L. V. Slipchenko, S. V. Levchenko, D. P. O'Neill, R. A. DiStasio Jr, R. C. Lochan, T. Wang, G. J. O. Beran, N. A. Besley, J. M. Herbert, C. Yeh Lin, T. Van Voorhis, S. Hung Chien, A. Sodt, R. P. Steele, V. A. Rassolov, P. E. Maslen, P. P. Korambath, R. D. Adamson, B. Austin, J. Baker, E. F. C. Byrd, H. Dachsel, R. J. Doerksen, A. Dreuw, B. D. Dunietz, A. D. Dutoi, T. R. Furlani, S. R. Gwaltney, A. Heyden, S. Hirata, C.-P. Hsu, G. Kedziora, R. Z. Khalliulin, P. Klunzinger, A. M. Lee, M. S. Lee, W. Liang, I. Lotan, N. Nair, B. Peters, E. I. Proynov, P. A. Pieniazek, Y. Min Rhee, J. Ritchie, E. Rosta, C. David Sherrill, A. C. Simmonett, J. E. Subotnik, H. Lee Woodcock, W. Zhang, A. T. Bell, A. K. Chakraborty, D. M. Chipman, F. J. Keil, A. Warshel, W. J. Hehre, H. F. Schaefer, J. Kong, A. I. Krylov, P. M. W. Gill and M. Head-Gordon, *Phys. Chem. Chem. Phys.*, 2006, **8**, 3172.
28 A. D. Becke, *J. Chem. Phys.*, 1993, **98**, 5648.
29 P. M. W. Gill, B. G. Johnson and J. A. Pople, *Chem. Phys. Lett.*, 1993, **209**, 506.
30 P. Pulay, *Chem. Phys. Lett.*, 1980, **73**, 393; P. Pulay, *J. Comput. Chem.*, 1982, **3**, 556.
31 A. J. H. Wachters, *J. Chem. Phys.*, 1970, **52**, 1033; C. W. Bauschlicher, S. R. Langhoff, H. Partridge and L. A. Barnes, *J. Chem. Phys.*, 1989, **91**, 2399.
32 R. Krishnan, J. S. Binkley, R. Seeger and J. A. Pople, *J. Chem. Phys.*, 1980, **72**, 650.
33 A. W. Lange and J. M. Herbert, *J. Chem. Phys.*, 2010, **133**, 244111; A. W. Lange and J. M. Herbert, *Chem. Phys. Lett.*, 2011, **509**, 77.
34 L. L. Tinker, N. D. McDaniel, P. N. Curtin, C. K. Smith, M. J. Ireland and S. Bernhard, *Chem.–Eur. J.*, 2007, **13**, 8726.

35 The reported one-pot method for step-wise nucleophilic aromatic substitutions of pyridine halides with alkylpyridines [A. Ünal, D. Wiedemann, J. Seiffert, J. P. Boyd and A. Grohmann, *Tetrahedron Lett.*, 2012, **53**, 54] can also be employed.
36 J. C. Knight, S. Alvarez, A. J. Amoroso, P. G. Edwards and N. Singh, *Dalton Trans.*, 2010, **39**, 3870.
37 S. Alvarez, D. Avnir, M. Llunell and M. Pinsky, *New J. Chem.*, 2002, **26**, 996; S. Alvarez, D. Avnir and P. Alemany, *Chem. Soc. Rev.*, 2005, **34**, 313; S. Alvarez, D. Avnir, P. Alemany, D. Casanova, M. Llunell and J. Cirera, *Coord. Chem. Rev.*, 2005, **249**, 1693; S. Alvarez, D. Avnir, M. Pinsky and M. Llunell, *Cryst. Eng.*, 2001, **4**, 179; M. Pinsky and D. Avnir, *Inorg. Chem.*, 1998, **37**, 5575; M. Pinsky, K. B. Lipkowitz and D. Avnir, *J. Math. Chem.*, 2001, **30**, 109.
38 J. M. Zadrozny, D. E. Freedman, D. M. Jenkins, T. D. Harris, A. T. Iavarone, C. Mathoniere, R. Clerac and J. R. Long, *Inorg. Chem.*, 2010, **49**, 8886.
39 C. Creutz, *Comments Inorg. Chem.*, 1982, **1**, 293.
40 (*a*) G. A. N. Felton, R. S. Glass, D. L. Lichtenberger and D. H. Evans, *Inorg. Chem.*, 2006, **45**, 9181; (*b*) V. Fourmond, P.-A. Jacques, M. Fontecave and V. Artero, *Inorg. Chem.*, 2010, **49**, 10338.
41 B. H. Solis and S. Hammes-Schiffer, *J. Am. Chem. Soc.*, 2011, **133**, 19036; B. H. Solis and S. Hammes-Schiffer, *J. Am. Chem. Soc.*, 2012, **134**, 15253.
42 CH_3CN binding to Co(I) has also experimentally been established: S. C. Marinescu, J. R. Winkler and H. B. Gray, *Proc. Natl. Acad. Sci. U. S. A.*, 2012, **109**, 15127.
43 R. S. Khnayzer, L. B. Thompson, M. Zamkov, S. Ardo, G. J. Meyer, C. J. Murphy and F. N. Castellano, *J. Phys. Chem. C*, 2012, **116**, 1429; X. H. Wang, S. Goeb, Z. Q. Ji, N. A. Pogulaichenko and F. N. Castellano, *Inorg. Chem.*, 2011, **50**, 705.
44 V. Artero and M. Fontecave, *Chem. Soc. Rev.*, 2013, **42**, 2338.
45 Y. Sun, J. Sun, J. R. Long, P. Yang and C. J. Chang, *Chem. Sci.*, 2013, **4**, 118.
46 B. Durham, J. V. Caspar, J. K. Nagle and T. J. Meyer, *J. Am. Chem. Soc.*, 1982, **104**, 4803; L. J. Henderson Jr, M. Ollino, V. K. Gupta, G. R. Newkome and W. R. Cherry, *J. Photochem.*, 1985, **31**, 199; T. K. Foreman, J. B. S. Bonilha and D. G. Whitten, *J. Phys. Chem.*, 1982, **86**, 3436.
47 N. Sutin and C. Creutz, in *Inorganic and Organometallic Photochemistry*, AMERICAN CHEMICAL SOCIETY, 1978, vol. 168, p. 1; C. R. Bock, J. A. Connor, A. R. Gutierrez, T. J. Meyer, D. G. Whitten, B. P. Sullivan and J. K. Nagle, *J. Am. Chem. Soc.*, 1979, **101**, 4815.